

Slow-light enhanced light-matter interactions with applications to gas sensing

K. H. Jensen

Center for Fluid Dynamics, Department of Micro and Nanotechnology, Technical University of Denmark, DTU Nanotech, Building 345 East, DK-2800 Kongens Lyngby, Denmark

M. N. Alam

Department of Chemical and Biochemical Engineering, Technical University of Denmark, DTU KT Building 227, DK-2800 Kongens Lyngby, Denmark

B. Scherer and A. Lambrecht

Fraunhofer Institute for Physical Measurement Techniques, Heidenhofstrasse 8, D-79110 Freiburg, Germany

N. A. Mortensen*

Department of Photonics Engineering, Technical University of Denmark, DTU Fotonik, Building 345 West, DK-2800 Kongens Lyngby, Denmark

Abstract

Optical gas detection in microsystems is limited by the short micron scale optical path length available. Recently, the concept of slow-light enhanced absorption has been proposed as a route to compensate for the short path length in miniaturized absorption cells. We extend the previous perturbation theory to the case of a Bragg stack infiltrated by a spectrally strongly dispersive gas with a narrow and distinct absorption peak. We show that considerable signal enhancement is possible. As an example, we consider a Bragg stack consisting of PMMA infiltrated by O₂. Here, the required optical path length for visible to near-infrared detection (~ 760 nm) can be reduced by at least a factor of 10^2 , making a path length of 1 mm feasible. By using this technique, optical gas detection can potentially be made possible in microsystems.

Key words:

PACS: 07.10.Cm, 42.62.-b, 42.25.Bs, 42.50.Gy, 42.68.Ca

1 Introduction

The integration of optics and microfluidics on lab-on-a-chip microsystems has recently been the topic of much research [1,2,3], partly motivated by its diverse applications in chemical and biochemical analysis [4]. The miniaturization of chemical analysis systems, however, presents many optical challenges since light-matter interactions suffer from the reduced optical path length L in lab-on-a-chip systems compared to their macroscopic counterparts as illustrated in Fig. 1. Mogensen *et al.* [5] demonstrated that for Beer–Lambert absorption measurements in a lab-on-a-chip system, a typical size reduction by two orders of magnitude severely reduces the optical sensitivity in an inversely proportional manner. This drawback is even more pronounced for gas detection in microsystems as most gases have a very weak absorption line. Thus, microsystems may not seem the obvious solution for gas sensing and detection. On the other hand, the major reason for being interested in pursuing microsystem opportunities is of course that many applications call for compact gas sensors because of limited sensor space. On the more practical level, we emphasize that lab-on-a-chip systems can both address very minute volumes (no flow), but also allows for measurements of larger volumes flowing through the microchannels where detection takes place. In that way, spatial variations in the gas properties can potentially be mapped onto a time axis and monitored through time-traces of the optical signal. This space-time mapping is a general approach (employed for a variety of other measurements) which is only possible in microchannels supporting laminar flow. For the optical sensitivity, it has been proposed, that by introducing a porous and strongly dispersive material, such as a photonic crystal, into the lab-on-a-chip microsystems one could potentially solve these problems through slow-light enhanced light-matter interactions [6,7,8,9]. First experimental evidence of this effect for gas sensors in the mid-infrared range was reported by Lambrecht *et al.* [10]. Here, we extend the perturbative theory in Refs. [6,7,8,9] to the case of a dispersive Bragg stack infiltrated by a spectrally strongly dispersive gas with a narrow and distinct absorption peak. We emphasize the example of oxygen monitoring and sensing based on the two distinctive bands near the visible to near-infrared light range of 760 nm referred to as the O₂ A band [11]. Spectral data are available from the HITRAN database [12]. Though, the A band has a very weak absorption feature, it offers the potential to establish an optical *in situ* O₂ detection for application in many fields including combustion processes [13] and fire research [14].

* Corresponding author

Email address: asger@mailaps.org (N. A. Mortensen).

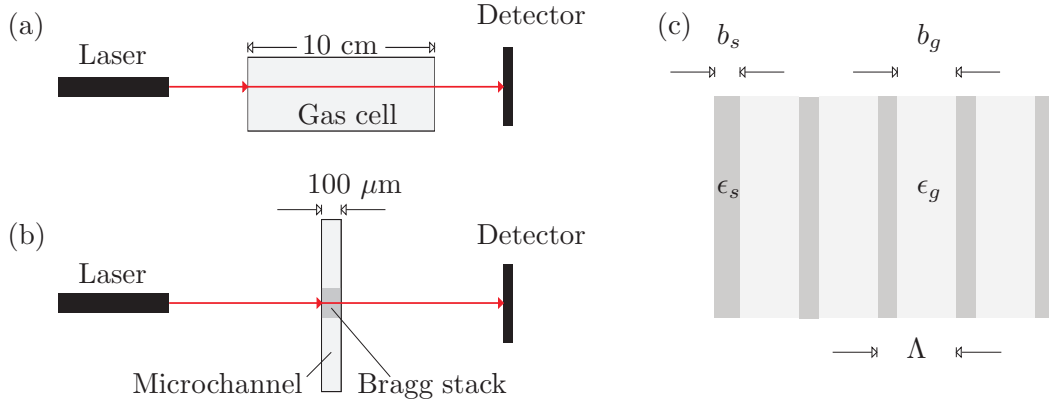


Fig. 1. (a) Schematic of a typical macroscopic gas detection setup with a light-matter interaction path length of 10 cm. (b) Schematic of a microscopic gas detection setup with a light-matter interaction path length of $100 \mu\text{m}$ made possible by the presence of a Bragg stack inside the microchannel. (c) Liquid/gas infiltrated Bragg stack composed of alternating solid and gas layers of thickness b_s and b_g , respectively.

2 Beer–Lambert absorption

In gas detection experiments, one typically uses Beer–Lambert absorption to determine the concentration of the substance of interest. As the light traverses the test chamber the light intensity is exponentially attenuated according to the relation

$$I = I_0 \exp(-\alpha L), \quad (1)$$

where α is the absorption coefficient, typically a linear function of the concentration \mathcal{C} of absorbing molecules (not to be confused with c ; the speed of light in vacuum to be introduced at a later stage). Any reduction in the optical path length L will penalize the sensitivity of the optical measurement significantly. However, by using a porous photonic crystal, it has been suggested that one may effectively enhance α by slowing down the light via a photonic crystal thereby overcoming the short path length obstacle in microsystems [6]. To quantify the enhancement, we shall use the ratio

$$\gamma = \frac{\Delta\alpha_{\text{pc}}}{\alpha_g}, \quad \Delta\alpha_{\text{pc}} = \alpha_{\text{pc}} - \lim_{\alpha_g \rightarrow 0} \alpha_{\text{pc}}, \quad (2)$$

where α_{pc} is the absorption coefficient inside the photonic crystal and α_g the corresponding homogeneous space absorption coefficient associated with the gas itself. The subscripts are introduced in order to carefully distinguish between absorption taking place in the photonic crystal material and the gas, respectively. In this work we consider the particular simple one-dimensional example of a Bragg stack and extend previous work [15] by using a more realistic model for the gas absorption profile.

3 The Bragg stack

The periodic Bragg stack is illustrated in panel (c) of Fig. 1 and is composed of alternating layers of gas and solid of thickness b_g and b_s , respectively. The lattice constant is $\Lambda = b_g + b_s$ and for the dielectric functions we allow for complex-valued bulk parameters, i.e. $\epsilon_g = \epsilon'_g + i\epsilon''_g$ and $\epsilon_s = \epsilon'_s + i\epsilon''_s$. For later convenience we rewrite the dielectric functions in terms of the bulk refractive index n and the damping coefficient α ,

$$\epsilon_g = n_g^2 + in_g\alpha_g/k, \quad (3a)$$

$$\epsilon_s = n_s^2 + in_s\alpha_s/k, \quad (3b)$$

where $k = 2\pi/\lambda = \omega/c$ is the free-space wave vector with λ being the corresponding free-space wavelength and ω the angular frequency. The dispersion relation for the Bragg stack is governed by (see Ref. [15] and references therein)

$$\cos(\kappa\Lambda) = F(k), \quad (4a)$$

where κ is the Bloch wave vector and

$$F(k) = \cos(\sqrt{\epsilon_g}kb_g) \cos(\sqrt{\epsilon_s}kb_s) - \frac{\epsilon_g + \epsilon_s}{2\sqrt{\epsilon_g\epsilon_s}} \sin(\sqrt{\epsilon_g}kb_g) \sin(\sqrt{\epsilon_s}kb_s). \quad (4b)$$

In the following we explicitly write the Bloch wave vector as $\kappa \equiv \kappa' + i\kappa''$, where κ' and κ'' are real and imaginary parts, respectively. The imaginary part causes an exponential damping of the Bloch states with a corresponding attenuation coefficient $\alpha_{pc} = 2\kappa''$. Likewise, in the homogeneous case we have $\alpha_g = k\epsilon''_g/\sqrt{\epsilon'_g}$ and in this way Eq. (2) now becomes

$$\gamma = \frac{2\sqrt{\epsilon'_g}}{\epsilon''_g} \times \frac{\kappa''(\epsilon''_s, \epsilon''_g) - \kappa''(\epsilon''_s, \epsilon''_g \rightarrow 0)}{k}. \quad (5)$$

If γ is greater than unity, it means that we have enhanced absorption due to the geometry of the Bragg stack. The absorption enhancement comes about because the group velocity of the light $\partial\omega/\partial\kappa'$ is reduced by the geometry of the Bragg stack [6]. In Eq. (5), the slow light phenomenon manifests itself through an increasing imaginary part of the Bloch vector κ'' as the band edge is approached. In deriving Eq. (5), we have separated the two different contributions to the absorption from the gas and the solid, thus implicitly assuming a small change in attenuation caused by the presence of the gas. However, we emphasize that the effect of material dispersion is included in the dispersion relation in an exact analytical and non-perturbative way and thus our results fulfill the Kramers–Kronig relation by taking the full interplay between waveguide and material dispersion into account.

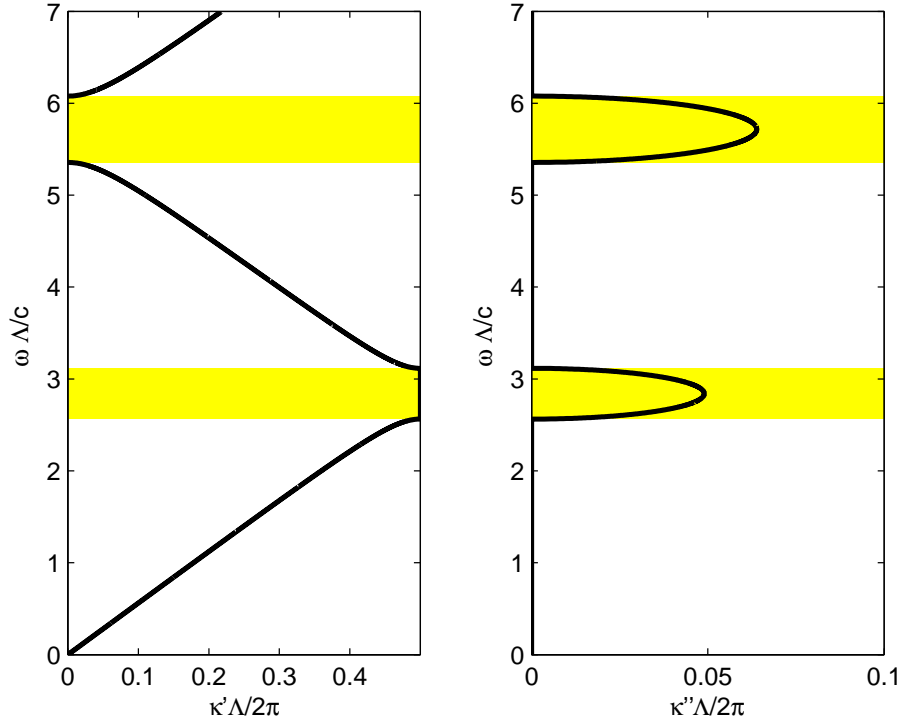


Fig. 2. Band diagram for a Bragg stack with $\epsilon_g = 1.0^2$, $\epsilon_s = 1.5^2$, $b_g = 0.8\Lambda$, and $b_s = 0.2\Lambda$, corresponding to a polymer infiltrated by gas.

4 Examples

In the following we illustrate the prospects for slow-light enhanced absorption by means of examples.

4.1 Non-absorbing materials

First, we consider the problem of two non-absorbing materials, say a gas and a polymer with $\epsilon_g = 1.0^2$ and $\epsilon_s = 1.5^2$. The corresponding band diagram, obtained from a numerical solution of Eq. (4a), is shown in Fig. 2. Two band gaps, indicated by yellow shading, are visible near $\omega\Lambda/c = 2.8$ and 5.5 . As can be seen, the group velocity approaches zero near the band gap edges while the imaginary part of κ attains a finite value only inside the band gaps where propagation of electromagnetic radiation is prohibited due to the exponential damping.

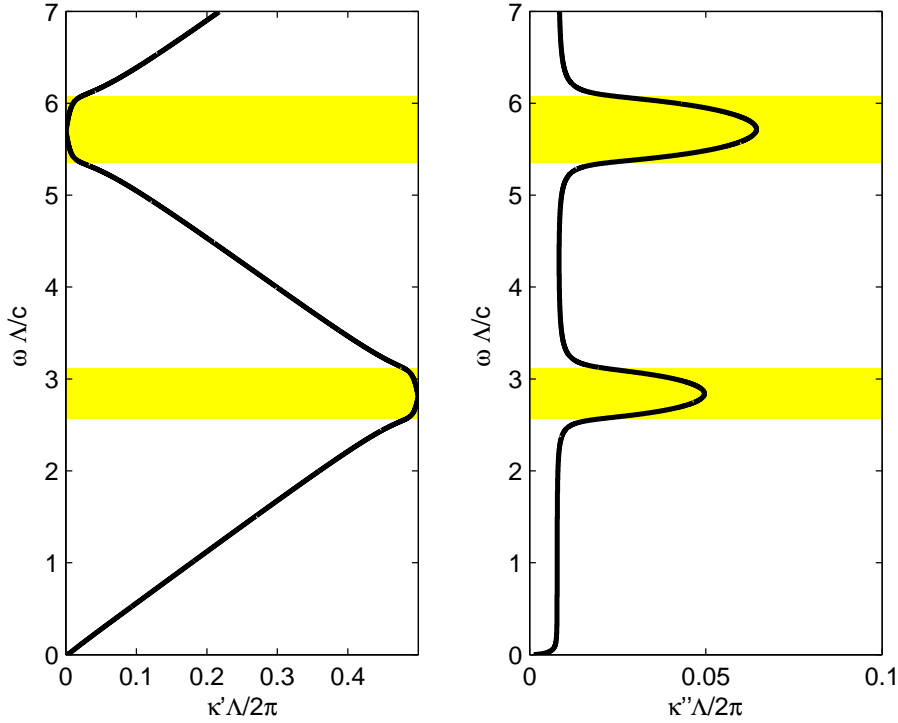


Fig. 3. Band diagram for the same problem as in Fig. 2, but with $\alpha_g \Lambda = \alpha_s \Lambda = 0.1$, corresponding to a finite bulk damping in the gas and the polymer, respectively.

4.2 Frequency-independent weakly absorbing materials

Next, we consider two weakly absorbing materials, say again the same gas and polymer, but now with imaginary contributions to the dielectric functions corresponding to damping parameters $\alpha_g \Lambda = \alpha_s \Lambda = 0.1$. As seen from the corresponding band diagram in Fig. 3, the main cause is to smear out the spectrally pronounced dispersion features. First, it increases κ'' from zero to a finite value outside the band gaps and second it smears out the band gap, setting a lower limit on the magnitude of the group velocity.

4.3 Strongly frequency-dependent absorbing gases

Having treated the simple case of spectrally uniform absorption, we shall now consider a slightly more realistic model for the frequency-dependent absorption in gasses. Due to causality and the Kramers–Kronig relation, the presence of frequency-dependent absorption is inevitably accompanied by material dispersion in the gas which will play in concert with the waveguide dispersion contributed by the geometry of the Bragg stack. To this end, we will now

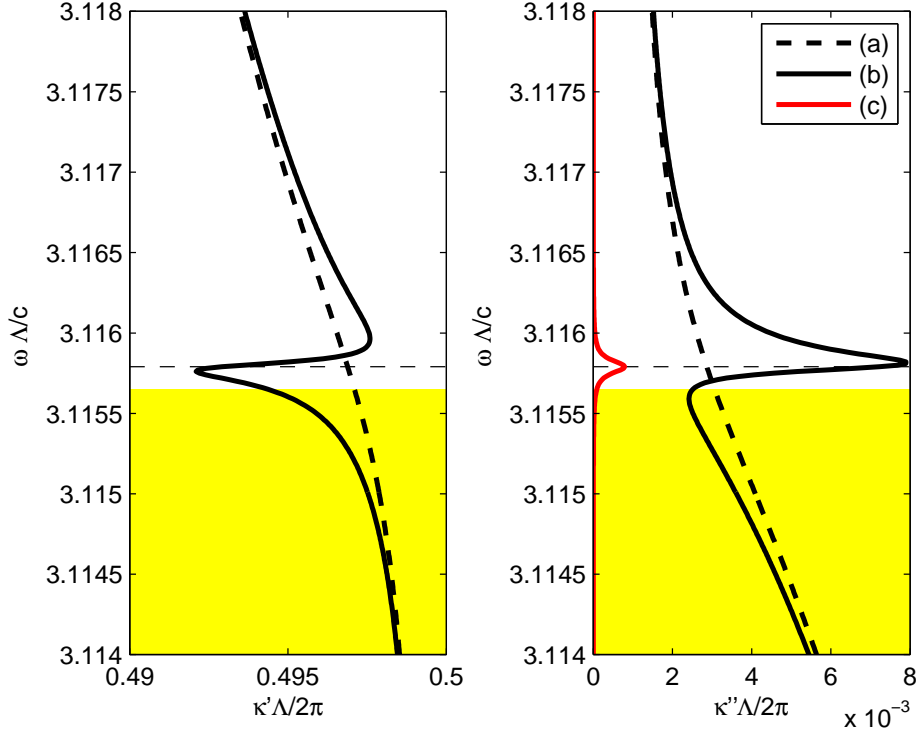


Fig. 4. Band diagram for a Bragg stack with $\alpha_s\Lambda = 0.1$, $n_s = 1.5$, $b_g = 0.8\Lambda$, $b_s = 0.2\Lambda$ and ϵ_g given by equations 6a-6b with $\omega_0\Lambda/c = 3.1158$, $\sigma\Lambda/c = 10^{-4}$ and $Ac^2/\Lambda^2 = 10^{-6}$. The black solid line (b) shows the results for the gas-infiltrated Bragg stack, while the corresponding dashed line (a) is in the absence of gas infiltration. In the κ'' plot, the red solid line (c) shows the absorption in the absence of the Bragg stack. Only the spectral region just above the band gap is emphasized in the plots.

consider a Lorentzian absorption line of the form [16]

$$\epsilon_g''(\omega) = A \frac{\sigma\omega}{(\omega^2 - \omega_0^2)^2 + \sigma^2\omega^2}, \quad (6a)$$

where the corresponding real part of the dielectric function follows from the Kramers–Kronig relation and is given by

$$\epsilon_g'(\omega) = 1 + A \frac{\omega_0^2 - \omega^2}{(\omega^2 - \omega_0^2)^2 + \sigma^2\omega^2}. \quad (6b)$$

In this model, the strength A scales with the concentration of molecules while σ quantifies the spectral line width around the resonance frequency ω_0 . As an example the band diagram for $\alpha_s\Lambda = 0.1$, $\omega_0\Lambda/c = 3.1158$, $\sigma\Lambda/c = 10^{-4}$, and $Ac^2/\Lambda^2 = 10^{-6}$ is shown in Fig. 4. Note the zoom-in on the first band gap and the different scale compared to Figs. 2 and 3. The horizontal dashed black line indicates the above-band-edge position of the absorption line while the yellow shading indicates the band gap for the absorption-free structure. The

red line shows bulk-absorption of the gas itself, thus indicating an absorption enhancement of the order $\gamma \simeq 5.5$. We emphasize that this value depends strongly on α_g , α_s , b_g , and b_s and as we shall see in the next section, even stronger absorption enhancement is possible by carefully tuning the Bragg stack parameters to fit the absorption line of interest.

5 Application to oxygen detection

Oxygen molecules, O_2 , exhibit a distinctive absorption band in the visible to near-infrared light range at 760 nm, which is called the Oxygen A band or the atmospheric transition of oxygen. These transitions are electric dipole forbidden, so only magnetic transitions are allowed, that require a change in the rotational quantum number of $dN = \pm 1$. Therefore the A-band splits in to the R-branch ($dN = -1$), starting at 759.8 nm with a bandwidth of 2.2 nm and the P-branch ($dN = +1$) starting at 762.3 nm with a bandwidth of 5.7 nm [17,11]. Though, the A band has a very weak absorption feature, it offers the potential to establish an optical *in situ* O_2 detection for a variety of applications, ranging from combustion processes [13] and fire research [14] to biomedical and environmental systems [18]. For this purpose different spectroscopic methods are used to enlarge the sensitivity of absorption measurements. Folding the laser beam several times in a multi reflection cell or using the long photon life times of high finesse cavities (cavity ring-down spectroscopy) offer an enhancement in sensitivity in respect to an enlargement of the absorption path length. In contrast, the method of slow light enhancement is related to an increased light matter interaction (though it may be phenomenologically explained as an enlarged effective path length), leading to higher absorption cross sections. This effect offers the potential for micrometer scaled probe volumes which is an important feature for e.g. lab on a chip applications. Typically, the absorption of oxygen in ambient air at the 760 nm line is of the order 2.6% with an optical path length of around 1 m [13]. At this wavelength, the O_2 absorption spectrum is minimally sensitive towards temperature changes and it is fairly influenced by the pressure variation [17,11,13]. The lowest oxygen concentration that can be measured is about 20-50 ppm which corresponds to transmission change of about 0.0005 [11]. The smallest experimentally detected absorption is about 3 times larger than the shot noise limit and is about 10^{-6} . This corresponds to a concentration of about 8 ppm at 1 m path length [19,20].

By extracting the spectroscopic data from the published works [13,14,21,22,23], we correlated the O_2 absorption coefficient, α [see Eq. (1)] as a function of O_2 concentration \mathcal{C} in the radiated volume. To lowest order in the gas concentration we expect that $\alpha(\mathcal{C}) = \eta\mathcal{C}$ and the linearity of the correlation obtained is shown in Fig. 5. The slope of the relatively linear line shows that it is possible

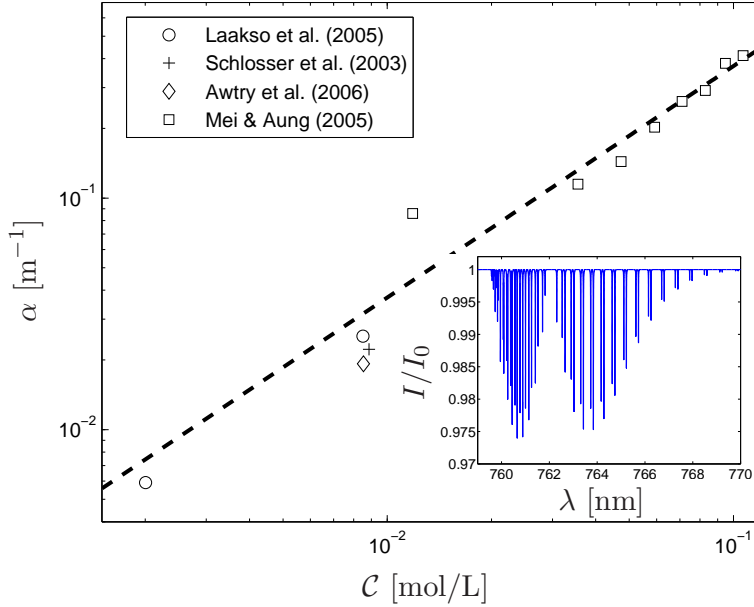


Fig. 5. O_2 absorption coefficient α as a function of the O_2 concentration C in the radiated volume. The inset shows the A band based on HITRAN data [12] for a path length of 1 m.

to obtain a fairly good measurement of O_2 molecule through the excitation of light at $\lambda \sim 760$ nm. From a linear fit we find that $\eta \sim 3.7 (\text{mol/L})^{-1}\text{m}^{-1}$. We note that the different absorption lines in the A-band have different line strengths which may cause the scatter of data in Fig. 5. The absorption in PMMA, at frequencies around the O_2 A band of oxygen, is fairly constant around $10/\text{m}$, i.e. of the order of 2.5×10^2 times stronger than the absorption in O_2 [24].

For the absorption coefficient in O_2 , we note that the 2.6% damping over one meter in the framework of Eq. (1) corresponds to $I/I_0 = 1 - 0.026 = \exp(-0.20942 \times \alpha_{O_2} \times 1 \text{ m})$ where we have explicitly accounted for the volume fraction of oxygen being 20.942% in ambient air. This translates into $\alpha_{O_2} = 0.126 \text{ m}^{-1}$ and for PMMA we have $\alpha_{\text{PMMA}} = 10 \text{ m}^{-1}$ while the corresponding dielectric functions are $\epsilon'_{O_2} = 1^2$ and $\epsilon'_{\text{PMMA}} = 1.5^2$. Choosing $\Lambda = 1 \mu\text{m}$ we find that the oxygen A band will be located right next to a band gap edge if we choose $b_g = 0.6262\Lambda$, resembling the situation shown in Fig. 4. Assuming a Lorentzian absorption profile and using the method discussed above, we find that $\gamma_{O_2} \simeq 235$. We emphasize that the Lorentzian linewidth correspond to the complete A band and thus resembles a group of different and even sharper absorption lines, see inset of Fig. 5, for which the enhance factor varies.

In a typical Beer–Lambert experiments measuring the O_2 concentration in the atmosphere, a path length of around 100 cm gives a 2.6% attenuation of the transmitted signal. The enhanced absorption in the Bragg stack dis-

cussed above implies that one could scale the path length down by a factor of $235 \frac{b_g}{\Lambda} \simeq 145$ to about 7 mm while retaining the same absorption signal. We emphasize that this sensitivity enhancement factor (effective path length/real length of the absorber) is even higher than that of a multi reflection cell, which is limited by reflection losses to about 100! Very high enhancement factors of 5 orders-of-magnitude or more compared to a single pass setup may be achieved using cavity-enhanced or cavity ringdown laser spectroscopy. However, such macrooptical setups can hardly be condensed into a microoptical device, and are generally delicate instruments mainly operated in laboratory environments. Using pairs of highly reflecting mirrors with reflectivities exceeding 99.999%, these setups are very sensitive to contamination e.g. by dust. In contrast the slow-light concept can be considered as a manifold of distributed mirrors. Hopefully, contamination shall not be as detrimental as with the macroscopic cavity approaches. In terms of bandwidth, the slow-light phenomenon shares physics with the various cavity-based approaches: strong enhancement of the absorption is obtained at the price of a narrow band-width!

6 Conclusion

Slow-light phenomena in photonic crystals has recently been proposed as a mechanism to allow for reduced path length in absorption measurements in microsystems. In this paper we have considered the effect an absorption line in a gas infiltrating a uniformly absorbing Bragg stack. We have shown that enhanced absorption is possible and as an example we have considered a Bragg stack consisting of PMMA infiltrated by O₂. In that case we have found the absorption enhancement to exceed a factor of 10² potentially allowing for O₂ detection with sub millimeter optical path lengths. For future directions we emphasize studies of the influence of the interfaces (scattering loss), structural imperfections, and beam divergence in more detail and another natural extension would be planar two-dimensional photonic crystals membranes.

Acknowledgement

We acknowledge Martin Heller and Henrik Bruus for useful discussions and technical assistance. Publication of this work is financially supported by the *Danish Research Council for Technology and Production Sciences* (grant no: 274-07-0080). KHJ acknowledges financial support by the *Danish National Research Foundation* (grant no: 74) and MNA is financially supported by *Universiti Teknologi Malaysia* and the *Malaysia Ministry of High Education*.

References

- [1] D. Erickson, Special issue on "optofluidics", *Microfluid. Nanofluid.* 4 (1-2) (2008) 1 – 2.
- [2] C. Monat, P. Domachuk, B. J. Eggleton, Integrated optofluidics: A new river of light, *Nature Photonics* 1 (2) (2007) 106 – 114.
- [3] D. Psaltis, S. R. Quake, C. H. Yang, Developing optofluidic technology through the fusion of microfluidics and optics, *Nature* 442 (7101) (2006) 381 – 386.
- [4] D. Janasek, J. Franzke, A. Manz, Scaling and the design of miniaturized chemical-analysis systems, *Nature* 442 (7101) (2006) 374 – 380.
- [5] K. B. Mogensen, J. El-Ali, A. Wolff, J. P. Kutter, Integration of polymer waveguides for optical detection in microfabricated chemical analysis systems, *Appl. Optics* 42 (19) (2003) 4072 – 4079.
- [6] N. A. Mortensen, S. Xiao, Slow-light enhancement of Beer-Lambert-Bouguer absorption, *Appl. Phys. Lett.* 90 (14) (2007) 141108.
- [7] J. Pedersen, N. A. Mortensen, Enhanced circular dichroism via slow light in dispersive structured media, *Appl. Phys. Lett.* 91 (21) (2007) 213501.
- [8] M. E. V. Pedersen, L. S. Rishøj, H. Steffensen, S. Xiao, N. A. Mortensen, Slow-light enhanced optical detection in liquid-infiltrated photonic crystals, *Opt. Quant. Electron.* 39 (10-11) (2007) 903 – 911.
- [9] N. A. Mortensen, S. Xiao, J. Pedersen, Liquid-infiltrated photonic crystals: enhanced light-matter interactions for lab-on-a-chip applications, *Microfluid. Nanofluid.* 4 (1-2) (2008) 117 – 127.
- [10] A. Lambrecht, S. Hartwig, S. L. Schweizer, R. B. Wehrspohn, Miniature infrared gas sensors using photonic crystals, *Proc. SPIE* 6480 (2007) 64800D.
- [11] B. Scherer, J. Wöllenstein, M. Weidemüller, W. Salzmann, J. M. Ostermann, F. Rinaldi, R. Michalzik, Measurement of the pressure broadening coefficients of the oxygen A-band using a low cost, polarization stabilized, widely tunable vertical-cavity surface-emitting laser, *Microsyst. Technol.* 14 (4-5) (2008) 607 – 614.
- [12] L. S. Rothman, D. Jacquemart, A. Barbe, D. C. Benner, M. Birk, L. R. Brown, M. R. Carleer, C. Chackerian, K. Chance, L. H. Coudert, V. Dana, V. M. Devi, J. M. Flaud, R. R. Gamache, A. Goldman, J. M. Hartmann, K. W. Jucks, A. G. Maki, J. Y. Mandin, S. T. Massie, J. Orphal, A. Perrin, C. P. Rinsland, M. A. H. Smith, J. Tennyson, R. N. Tolchenov, R. A. Toth, J. Vander Auwera, P. Varanasi, G. Wagner, The HITRAN 2004 molecular spectroscopic database, *J. Quant. Spectrosc. Radiat. Transf.* 96 (2) (2005) 139 – 204.
- [13] H. E. Schlosser, J. Wolfrum, V. Ebert, B. A. Williams, R. S. Sheinson, J. W. Fleming, In situ determination of molecular oxygen concentrations in full-scale

- fire-suppression tests using tunable diode laser absorption spectroscopy, *Proc. Combust. Inst.* 29 (2003) 353 – 360.
- [14] M. Laakso, M. Jalonen, S. Laukkanen, A compact ruggedized tuneable diode laser spectrometer for oxygen sensing, *Technical Papers of The Instrumentation, Systems and Automation Society* 459 (2005) 1178–1188.
- [15] J. Pedersen, S. Xiao, N. A. Mortensen, Slow-light enhanced absorption for biochemical sensing applications: potential of low-contrast lossy materials, *J. Eur. Opt. Soc., Rapid Publ.* 3 (2008) 08007.
- [16] D. J. Griffiths, *Introduction to Electrodynamics*, 3rd Edition, Prentice Hall, Upper Saddle River, New Jersey, 1999.
- [17] L. R. Brown, C. Plymate, Experimental line parameters of the oxygen A band at 760 nm, *J. Mol. Spectrosc.* 199 (2) (2000) 166 – 179.
- [18] S. Raab, K. Hoffmann, M. Gabbert, M. V. Glushkov, Y. V. Kosichkin, Application of a diode laser with an external resonator in high resolution spectroscopy, *Sov. J. Quantum Electron.* (8) (1981) 1068–1071.
- [19] P. Vogel, V. Ebert, Near shot noise detection of oxygen in the A-band with vertical-cavity surface-emitting lasers, *Appl. Phys. B-Lasers Opt.* 72 (1) (2001) 127 – 135.
- [20] P. Werle, F. Slemr, M. Gehrtz, C. Brauchle, Quantum-limited FM-spectroscopy with a lead-salt diode-laser: A comparison of theoretical and experimental data, *Appl. Phys. B* 49 (2) (1989) 99 – 108.
- [21] D. J. Robichaud, J. T. Hodges, L. R. Brown, D. Lisak, P. Maslowski, L. Y. Yeung, M. Okumura, C. E. Miller, Experimental intensity and lineshape parameters of the oxygen A-band using frequency-stabilized cavity ring-down spectroscopy, *J. Mol. Spectrosc.* 248 (1) (2008) 1 – 13.
- [22] A. R. Awtry, J. W. Fleming, V. Ebert, Simultaneous diode-laser-based in situ measurement of liquid water content and oxygen mole fraction in dense water mist environments, *Opt. Lett.* 31 (7) (2006) 900–902.
- [23] A. Mei, K. Aung, A method for stimulating and measuring the concentration of oxygen by absorption laser spectroscopy, *Proc. IMECE* (2005) 356–370.
- [24] G. Khanarian, H. Celanese, Optical properties of cyclic olefin copolymers, *Opt. Eng.* 40 (6) (2001) 1024 – 1029.